Author's Accepted Manuscript

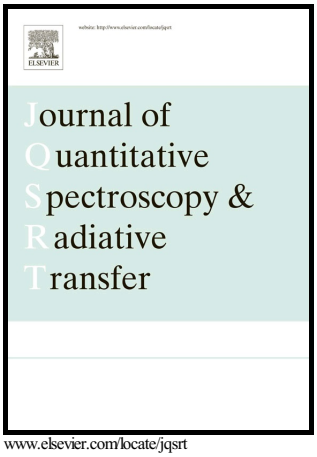

www.elsevier.com/locate/jqsrt

Applicability of the effective-medium approximation to heterogeneous aerosol particles

Michael I. Mishchenko, Janna M. Dlugach, Li Liu

PII: S0022-4073(15)30279-X
DOI: http://dx.doi.org/10.1016/j.jqsrt.2015.12.028
Reference: JQSRT5173

To appear in: *Journal of Quantitative Spectroscopy and Radiative Transfer*

Received date: 1 December 2015
Accepted date: 25 December 2015

Cite this article as: Michael I. Mishchenko, Janna M. Dlugach and Li Liu Applicability of the effective-medium approximation to heterogeneous aerosol particles, *Journal of Quantitative Spectroscopy and Radiative Transfer*, http://dx.doi.org/10.1016/j.jqsrt.2015.12.028

Applicability of the effective-medium approximation to heterogeneous aerosol particles

Michael I. Mishchenko[a,*], Janna M. Dlugach[b], Li Liu[a,c]

[a]*NASA Goddard Institute for Space Studies, 2880 Broadway, New York, NY 10025, USA*

[b]*Main Astronomical Observatory of the National Academy of Sciences of Ukraine, 27 Zabolotny Str., 03680, Kyiv, Ukraine*

[c]*Department of Applied Physics and Applied Mathematics, Columbia University, 2880 Broadway, New York, NY 10025, USA*

[*]Correspondence to: M. I. Mishchenko (michael.i.mishchenko@nasa.gov)

Abstract

The effective-medium approximation (EMA) is based on the assumption that a heterogeneous particle can have a homogeneous counterpart possessing similar scattering and absorption properties. We analyze the numerical accuracy of the EMA by comparing superposition *T*-matrix computations for spherical aerosol particles filled with numerous randomly distributed small inclusions and Lorenz–Mie computations based on the Maxwell-Garnett mixing rule. We verify numerically that the EMA can indeed be realized for inclusion size parameters smaller than a threshold value. The threshold size parameter depends on the refractive-index contrast between the host and inclusion materials and quite often does not exceed several tenths, especially in calculations of the scattering matrix and the absorption cross section. As the inclusion size parameter approaches the threshold value, the scattering-matrix errors of the EMA start to grow with increasing the host size parameter and/or the number of inclusions. We confirm, in particular, the existence of the effective-medium regime in the important case of dust aerosols with hematite or air-bubble inclusions, but then the large refractive-index contrast necessitates inclusion size parameters of the order of a few tenths. Irrespective of the highly restricted conditions of applicability of the EMA, our results provide further evidence that the effective-medium regime must be a direct corollary of the macroscopic Maxwell equations under specific assumptions.

Keywords:
Scattering
Effective-medium approximation
Heterogeneous aerosols
Mineral dust
T-matrix method

1. Introduction

Owing to its unparalleled simplicity, the effective-medium approximation (EMA) has been widely used to model complex heterogeneous substances as being homogeneous and having a refractive index computed with one of the phenomenological mixing rules such as the Lorentz–Lorenz, Bruggeman, and Maxwell-Garnett formulas [1,2]. Applications of various mixing rules in remote sensing, atmospheric radiation, and climate modeling research have been so ubiquitous that it would hardly be possible to assemble a representative list of relevant publications as it would contain hundreds of entries.

The use of the EMA appears to be unavoidable in many cases given the extreme morphological complexity of the vast majority of aerosol particles (e.g., [3–12]). The main cause of this situation is the limited applicability of direct computer solvers of the Maxwell equations to representative ensembles of heterogeneous particles. It should be kept in mind however that, in the words of Chýlek et al. [2], mixing rules have always been heuristic shortcuts not derived explicitly from the Maxwell equations. As a consequence, the accuracy of such *ad hoc* effective refractive indices (ERIs) and the precise conditions for their permissible use have often been difficult to assess.

Despite the obvious shortcomings of the EMA, its applications in remote sensing and climate research can be expected to be as widespread in the future as they have been in the past. For example, the use of the concept of an ERI has been and is expected to remain *implicit* in virtually all computations of electromagnetic scattering by dust-like aerosols since it has become the norm to ignore the internal heterogeneity of such particles. Therefore, the failure of this concept in application to dust-like aerosols may create an extremely problematic situation. This makes it imperative to perform an in-depth analysis of the range and conditions of practical applicability of the EMA.

This analysis has been initiated in several recent publications [13–18] by taking advantage of the latest improvements in first-principle modeling methodologies [19]. The overall outcome of these studies can hardly be characterized as optimistic. It should be recognized however that some of these initial results are based on a few rather artificial models of heterogeneous aerosols that do not necessarily offer the EMA a "fair chance". Indeed, it is well known that the concept of bulk refractive index is a byproduct of deriving the macroscopic Maxwell equations from the microscopic Maxwell–Lorentz equations dealing with discrete elementary charges [20–30]. The main assumption in this derivation is that the microscopic electromagnetic field can be meaningfully homogenized over "physically infinitesimal" volume elements that are much smaller than the wavelength and yet contain vast numbers of molecules. It is obvious that the extrapolation of this approach to the case of a macroscopically heterogeneous material must also be based on the assumption that inclusions are quasi-uniformly distributed throughout the host medium, are sufficiently small, and are present in large numbers. Only then can one hope that the concept of the ERI might work.

We have already mentioned that a direct *analytical* derivation of the EMA from the Maxwell equations is still absent. However, the actual existence of the effective-medium regime has been demonstrated *numerically* by comparing Lorenz–Mie results for a homogeneous spherical particle with those obtained by applying the superposition *T*-matrix solver of the Maxwell equations to a spherical particle filled randomly with a large number of very small spherical inclusions [31]. The refractive indices of the host and of the inclusions were 1.33 and 1.55, respectively. The possibility to identify an ERI enabling the Lorenz–Mie theory to reproduce even the finest details of the angular profile of the scattering matrix demonstrated convincingly that the effective-medium concept must have physical validity. Yet the practical range of this validity may not necessarily be wide and may exclude many actual types of heterogeneous atmospheric particulates.

Given the great importance of mineral-dust aerosols in atmospheric radiative-transfer modeling and remote sensing, the main objective of this paper is to extend the analysis of [31] and demonstrate numerically the fundamental existence of the effective-medium regime in the case of two types of inclusions representing the largest refractive-index contrast with the mineral host, i.e., air bubbles and absorbing hematite grains. Furthermore, we trace and analyze the accumulation of errors of the EMA as the ideal conditions of the ERI regime are

increasingly violated. A useful intermediate aspect of our study is a general analysis of the accuracy of the EMA as a function of the inclusion size parameter and of the refractive-index contrast between the host particle and the inclusions.

2. Modeling methodology

The gist of the EMA is illustrated in Fig. 1 wherein a particle randomly filled with numerous, quasi-uniformly distributed small inclusions is replaced by a homogeneous object of the same overall shape but with an artificial (effective) refractive index coinciding neither with that of the host nor with that of the inclusions. Given its artificial nature, the ERI carries no independent physical content and is useful only to the extent to which it can simplify the computation of relevant optical observables. In the case of atmospheric radiative-transfer and remote-sensing research, all such observables can, in the final analysis, be expressed in terms of the elements of the real-valued 4×4 so-called phase and extinction matrices $\mathbf{Z}(\hat{\mathbf{n}}^{\rm sca}, \hat{\mathbf{n}}^{\rm inc})$ and $\mathbf{K}(\hat{\mathbf{n}}^{\rm inc})$ [32,33]. These matrices provide a self-contained description of electromagtnetic scattering in the far zone of a finite object illuminated by a plane electromagnetic wave incident in the direction of the unit vector $\hat{\mathbf{n}}^{\rm inc}$, the unit vector $\hat{\mathbf{n}}^{\rm sca}$ specifying the scattering direction. The computation of these matrices and/or appropriate derivative quantities using various mixing rules and a direct computer solver of the Maxwell equations thus serves as a suitable means of evaluating the accuracy of the EMA.

In many cases aerosol particles have nonspherical outer boundaries in addition to being internally heterogeneous. In principle, realistic computations of electromagnetic scattering by such aerosols should be based on particle models incorporating both morphological features. It should be kept in mind however that the effects of nonsphericity and internal heterogeneity on the phase and extinction matrices can be similar, thereby making it problematic to evaluate unequivocally the actual performance of a mixing rule intended to simulate only the effects of internal heterogeneity. To circumvent this problem, we will model atmospheric aerosols as particles with spherical overall shapes (see the upper panel of Fig. 1). An added benefit of this approach is the possibility to use the highly efficient and accurate superposition *T*-matrix method (STMM) with its quasi-analytical orientation-averaging procedure [34,35].

By its very nature, the EMA is intended to reproduce the scattering and absorption

properties of particles with heterogeneous yet statistically uniform interiors [1,2]. We simulate the statistical randomness and quasi-uniformity of a heterogeneous particle's interior in two steps. First, we use a random-number generator to create a fixed yet quasi-random configuration of a large number N of inclusions, while making sure that the volumes of the inclusions do not overlap and do not cross the particle's outer boundary. Second, we average the relevant far-field optical observables over the equiprobable orientation distribution of the resulting discretely heterogeneous object using the STMM code described by Mackowski [35]. In principle, this procedure should be repeated a number of times for different randomly generated configurations of the N inclusions, and the resulting optical observables should be configuration-averaged. However, several control tests have shown that averaging over different configurations of inclusions is not essential since the final result is virtually indistinguishable from that obtained by using only one randomly generated configuration.

Quite a number of mixing rules have been proposed over the years, as summarized by Sihvola [1] and Chýlek et al. [2]. Evaluating all of them one-by-one can be exceedingly laborious, but is hardly needed. Indeed, we have verified that in all specific cases considered below, the popular Maxwell-Garnett (MG) and Bruggemann mixing rules yield very close (if not nearly identical) ERIs. Therefore, all our results and conclusions apply equally to both mixing rules. Furthermore, our previous studies [31,36] as well as extensive additional tests (not shown) have demonstrated that if the STMM result for a heterogeneous particle can be accurately reproduced by a Lorenz–Mie computation then the resulting best-fit ERI is likely to be very close to the MG ERI. Based on this evidence, we will narrow the scope of our study by evaluating the performance of only the MG mixing rule.

In this paper we will analyze only light scattering by randomly oriented particles, which makes it a convenient simplification to assume that $\hat{\mathbf{n}}^{\rm inc}$ points in the positive direction of the z-axis of the laboratory spherical coordinate system. The scattering geometry can thus be summarized by Fig. 2. It is worth reminding that the introduction of the far-field phase and extinction matrices is based on the assumption that the Stokes parameters of the incident plane wave and the outgoing spherical scattered wave are defined with respect to the corresponding meridional planes containing the vectors $\hat{\mathbf{n}}^{\rm inc}$ and $\hat{\mathbf{n}}^{\rm sca}$ as well as the z-axis. Since $\hat{\mathbf{n}}^{\rm inc}$ is parallel to the z-axis, there is no implicit meridional plane of the incident light. Therefore, this plane must be prescribed explicitly.

For demonstration purposes, we define the 4×4 dimensionless scattering matrix

$\widetilde{\mathbf{F}}(\Theta)$ according to

$$\widetilde{\mathbf{F}}(\Theta) = \frac{4\pi}{C_{\rm sca}} \langle \mathbf{Z}(\theta^{\rm sca} = \Theta, \varphi^{\rm sca}; \theta^{\rm inc} = 0, \varphi^{\rm inc} = \varphi^{\rm sca}; \Psi) \rangle_{\Psi}, \quad (1)$$

where $\theta \in [0, \pi]$ is the polar angle of a propagation direction, $\varphi \in [0, 2\pi)$ is the corresponding azimuth angle, and Θ is the scattering angle; the average is taken over the equiprobable distribution of orientations Ψ of a heterogeneous particle; and the normalization constant $C_{\rm sca}$ is given by

$$C_{\rm sca} = \int_{4\pi} {\rm d}\hat{\mathbf{n}}^{\rm sca} \langle Z_{11}(\theta^{\rm sca}, \varphi^{\rm sca}; \theta^{\rm inc} = 0, \varphi^{\rm inc} = 0; \Psi) \rangle_{\Psi}. \quad (2)$$

Note that the uniform orientation distribution renders $\widetilde{\mathbf{F}}$ independent of $\varphi^{\rm sca}$, while $C_{\rm sca}$ represents the orientation-averaged scattering cross section for the particular case of unpolarized incident light [32,33]. The $(1,1)$ element of the scattering matrix $\widetilde{\mathbf{F}}(\Theta)$ (traditionally called the phase function) is normalized according to

$$\frac{1}{2} \int_0^{\pi} {\rm d}\Theta \sin\Theta \, \widetilde{F}_{11}(\Theta) = 1. \quad (3)$$

A frequently used far-field scattering characteristic is the so-called asymmetry parameter defined as

$$g = \frac{1}{2} \int_0^{\pi} {\rm d}\Theta \sin\Theta \, \widetilde{F}_{11}(\Theta) \cos\Theta. \quad (4)$$

Owing to the uniform orientation distribution, the dimensionless scattering matrix (1) has the following well-known symmetric structure [32,37]:

$$\widetilde{\mathbf{F}}(\Theta) = \begin{bmatrix} \widetilde{F}_{11}(\Theta) & \widetilde{F}_{21}(\Theta) & \widetilde{F}_{13}(\Theta) & \widetilde{F}_{14}(\Theta) \\ \widetilde{F}_{21}(\Theta) & \widetilde{F}_{22}(\Theta) & \widetilde{F}_{23}(\Theta) & \widetilde{F}_{24}(\Theta) \\ -\widetilde{F}_{13}(\Theta) & -\widetilde{F}_{23}(\Theta) & \widetilde{F}_{33}(\Theta) & \widetilde{F}_{34}(\Theta) \\ \widetilde{F}_{14}(\Theta) & \widetilde{F}_{24}(\Theta) & -\widetilde{F}_{34}(\Theta) & \widetilde{F}_{44}(\Theta) \end{bmatrix}. \quad (5)$$

Numerous STMM computations for heterogeneous spherical particles with multiple quasi-randomly distributed inclusions have demonstrated that the elements populating the upper right and lower left 2×2 blocks of this matrix are negligibly small (in the absolute-value sense) compared to the other elements. This is an expected result of averaging over the

equiprobable orientation distribution of an inhomogeneous particle coupled with quasi-randomness of the initial inclusion positions throughout the particle volume. Thus the scattering matrix can be considered to have the following typical block-diagonal structure:

$$\widetilde{\mathbf{F}}(\Theta) \approx \begin{bmatrix} \widetilde{F}_{11}(\Theta) & \widetilde{F}_{21}(\Theta) & 0 & 0 \\ \widetilde{F}_{21}(\Theta) & \widetilde{F}_{22}(\Theta) & 0 & 0 \\ 0 & 0 & \widetilde{F}_{33}(\Theta) & \widetilde{F}_{34}(\Theta) \\ 0 & 0 & -\widetilde{F}_{34}(\Theta) & \widetilde{F}_{44}(\Theta) \end{bmatrix}. \tag{6}$$

A fundamental property of the Lorenz–Mie (LM) scattering matrix is the identity [37]

$$\widetilde{F}_{22}^{\mathrm{LM}}(\Theta) \equiv \widetilde{F}_{11}^{\mathrm{LM}}(\Theta). \tag{7}$$

This implies that if the boundary of a host particle is perfectly spherical then the EMA yields this identity precisely, irrespective of the actual particle interior. Therefore, a deviation of the ratio $\widetilde{F}_{22}(\Theta)/\widetilde{F}_{11}(\Theta)$ for a heterogeneous spherical object from 100% serves as the most direct and unequivocal indicator of the numerical failure of the EMA [13,31].

The extinction matrix also becomes simpler upon averaging over the equiprobable orientation distribution of a heterogeneous particle. Specifically, it becomes independent of $\hat{\mathbf{n}}^{\mathrm{inc}}$ and has the following symmetric form [33]:

$$\langle \mathbf{K}(\hat{\mathbf{n}}^{\mathrm{inc}}; \Psi) \rangle_{\Psi} = \begin{bmatrix} K_{11} & 0 & 0 & K_{14} \\ 0 & K_{11} & K_{23} & 0 \\ 0 & -K_{23} & K_{11} & 0 \\ K_{14} & 0 & 0 & K_{11} \end{bmatrix}. \tag{8}$$

Furthermore, the off-diagonal elements become negligibly small in comparison to the diagonal ones, so that the extinction matrix can be considered to be diagonal and given by

$$\langle \mathbf{K}(\hat{\mathbf{n}}^{\mathrm{inc}}; \Psi) \rangle_{\Psi} \approx C_{\mathrm{ext}} \begin{bmatrix} 1 & 0 & 0 & 0 \\ 0 & 1 & 0 & 0 \\ 0 & 0 & 1 & 0 \\ 0 & 0 & 0 & 1 \end{bmatrix}, \tag{9}$$

where C_{ext} is the orientation-averaged extinction cross section.

3. Accuracy of the EMA as a function of the inclusion size parameter and relative refractive index

By analogy with the well-known Rayleigh approximation [37], we can expect that the accuracy of the EMA must depend strongly on the size parameter of the inclusions and their refractive index relative to that of the host particle. To demonstrate the effect of the refractive-index contrast, in Fig. 3 we depict three errors of the MG mixing rule defined according to

$$\delta\widetilde{F}_{11}(\Theta) = \left|\frac{\widetilde{F}_{11}^{\mathrm{MG}}(\Theta) - \widetilde{F}_{11}^{\mathrm{STMM}}(\Theta)}{\widetilde{F}_{11}^{\mathrm{MG}}(\Theta)}\right| \times 100\%, \tag{10}$$

$$\delta\widetilde{F}_{21}(\Theta) = \left|\frac{\widetilde{F}_{21}^{\mathrm{MG}}(\Theta)}{\widetilde{F}_{11}^{\mathrm{MG}}(\Theta)} - \frac{\widetilde{F}_{21}^{\mathrm{STMM}}(\Theta)}{\widetilde{F}_{11}^{\mathrm{STMM}}(\Theta)}\right| \times 100\%, \tag{11}$$

$$\delta\widetilde{F}_{34}(\Theta) = \left|\frac{\widetilde{F}_{34}^{\mathrm{MG}}(\Theta)}{\widetilde{F}_{11}^{\mathrm{MG}}(\Theta)} - \frac{\widetilde{F}_{34}^{\mathrm{STMM}}(\Theta)}{\widetilde{F}_{11}^{\mathrm{STMM}}(\Theta)}\right| \times 100\%. \tag{12}$$

These errors were calculated assuming the following fixed values of the heterogeneous-particle characteristics: the host size parameter $X = 2\pi R/\lambda = 10$, where R is the host-particle radius and λ is the wavelength of the incident light; the host refractive index $m_{\mathrm{host}} = 1.32$; the inclusion size parameter $x = 2\pi r/\lambda = 0.3$, where r is the inclusion radius; and the number of inclusions $N = 8000$. The resulting volume fraction of the inclusions is 21.6%. The only variable characteristic was the inclusion refractive index m_{incl} which ranged from 1.4 to 2 while remaining real-valued. Table 1 lists the corresponding extinction and asymmetry-parameter errors defined by

$$\delta C_{\mathrm{ext}} = \frac{C_{\mathrm{ext}}^{\mathrm{MG}} - C_{\mathrm{ext}}^{\mathrm{STMM}}}{C_{\mathrm{ext}}^{\mathrm{MG}}} \times 100\%, \tag{13}$$

$$\delta g = \frac{g^{\mathrm{MG}} - g^{\mathrm{STMM}}}{g^{\mathrm{MG}}} \times 100\%, \tag{14}$$

while panels a–g of Fig. 4 depict the corresponding angular profiles of the ratio $\widetilde{F}_{22}^{\mathrm{STMM}}(\Theta)/\widetilde{F}_{11}^{\mathrm{STMM}}(\Theta)$. Note that since the refractive indices of both the host and the inclusions are real-valued, the scattering cross section coincides with the extinction cross section: $C_{\mathrm{sca}} = C_{\mathrm{ext}}$.

Figure 3 demonstrates that if the refractive index of the host-particle material and that

of the inclusions are very close (1.32 and 1.4, respectively) then all three errors are negligibly small. As expected, the errors grow with increasing refractive-index contrast between the host and the inclusions. This growth is not always monotonous at all scattering angles, yet by the time the refractive index of the inclusions reaches the value 2, all three errors exhibit values that can be considered unacceptable in many applications. Importantly, this happens despite the very small size parameter of the inclusions. The deviation of the ratio $\widetilde{F}_{22}^{\mathrm{STMM}}(\Theta)/\widetilde{F}_{11}^{\mathrm{STMM}}(\Theta)$ from 100% in Figs. 4a–g also increases with increasing refractive-index contrast and reaches 10% for $m_{\mathrm{incl}} = 2$. Again, this is a qualitatively expected result.

The results shown in Table 1 reveal that the extinction and asymmetry-parameter errors of the MG mixing rule are substantially smaller than the scattering-matrix errors. They do seem to increase with m_{incl}, but remain sufficiently small for most typical applications.

Panels h–l of Fig. 4 reveal other interesting traits of the ratio $\widetilde{F}_{22}^{\mathrm{STMM}}(\Theta)/\widetilde{F}_{11}^{\mathrm{STMM}}(\Theta)$ which suggest that the errors of the MG mixing rule can depend in a rather convoluted way on the inclusion number, size parameter, and refractive-index contrast. First, Fig. 4h pertains to the case of $N = 8000$ air-bubble inclusions with $m_{\mathrm{incl}} = 1$ and $x = 0.3$. The corresponding refractive-index contrast is similar to that in the case of $m_{\mathrm{incl}} = 1.75$. However, comparison of Fig. 4h with Figs. 4d,e shows significantly smaller deviations of the ratio $\widetilde{F}_{22}^{\mathrm{STMM}}(\Theta)/\widetilde{F}_{11}^{\mathrm{STMM}}(\Theta)$ from 100% in the former case. The cause of this disparity is not immediately obvious to us.

Second, comparison of panels g, i, and j of Fig. 4 shows that in the high-contrast case of $m_{\mathrm{incl}} = 2$, the performance of the MG mixing rule deteriorates rather strongly as the number of inclusions increases. Interestingly, this deterioration is virtually absent in the low-contrast case of $m_{\mathrm{incl}} = 1.4$ (not shown).

Third, comparison of Figs. 4a and 4k as well as of Figs. 4j and 4l shows that decreasing the inclusion size parameter while keeping their volume fraction fixed can result in a significant (if not dramatic) reduction of errors of the MG mixing rule. The same conclusion follows from comparing the first and last entries of Table 1.

4. Dust-like aerosols with hematite and air-bubble inclusions

Following Kahnert [16], we use $m_{\mathrm{host}} = 1.6$ as the generic refractive index of the dust-

particle host material. According to Table 1 of Lindqvist et al. [38], the refractive indices of the majority of materials encountered in dust aerosols are within several hundredths of the generic value and thus represent the case of low refractive-index contrast. Major exceptions are the cases of hematite ($m_{\rm incl}$ = 3.102 + i0.0925) and air-bubble ($m_{\rm incl}$ = 1) inclusions which require a special consideration.

As before, we assume that a spherical dust particle is filled with identical spherical inclusions. The size parameter of the spherical host is fixed at either X = 4 or 8, while the number N of inclusions varies with the inclusion size parameter x such that the cumulative volume fraction of the inclusions remains fixed at 2%. According to Lindqvist et al. [38], the 2% volume fraction is typical of the hematite content in dust aerosols. Table 2 along with Figs. 5 and 6 summarize the results of computations for dust particles with hematite inclusions, while Table 3 along with Figs. 7 and 8 summarize those for dust particles with air-bubble inclusions. The corresponding MG refractive indices are 1.6231 + i0.9779×10^{-3} and 1.5878. Note that the errors $\delta C_{\rm sca}$, $\delta C_{\rm abs}$, and $\delta\varpi$ are defined by analogy with Eqs. (13) and (14):

$$\delta C_{\rm sca} = \frac{C_{\rm sca}^{\rm MG} - C_{\rm sca}^{\rm STMM}}{C_{\rm sca}^{\rm MG}} \times 100\%, \tag{15}$$

$$\delta C_{\rm abs} = \frac{C_{\rm abs}^{\rm MG} - C_{\rm abs}^{\rm STMM}}{C_{\rm abs}^{\rm MG}} \times 100\%, \tag{16}$$

$$\delta\varpi = \frac{\varpi^{\rm MG} - \varpi^{\rm STMM}}{\varpi^{\rm MG}} \times 100\%, \tag{17}$$

where

$$C_{\rm abs} = C_{\rm ext} - C_{\rm sca} \geq 0 \tag{18}$$

is the (non-negative) absorption cross section and

$$\varpi = \frac{C_{\rm sca}}{C_{\rm ext}} \leq 1 \tag{19}$$

is the single-scattering albedo. Obviously, it is the presence of absorbing hematite inclusions that causes the inequalities $C_{\rm abs} > 0$ and $\varpi < 1$.

The most profound outcome of these computations is the quantitative demonstration

of the existence of the effective-medium regime for dust aerosols filled with hematite or air-bubble inclusions. Indeed, the red curves in Figs. 5–8 essentially occult the black curves depicting the corresponding MG results and thereby reproduce even the finest angular features of the MG scattering matrix. This implies that the inclusion size parameters $x = 0.1$ for hematite and 0.15 for air bubbles are definitely within the EMA domain.

However, the inclusion size parameter $x = 0.5$ is already outside the EMA domain. Indeed, the phase-function errors of the MG mixing rule can now exceed a factor of three, while the ratio $\widetilde{F}_{22}^{\rm STMM}(\Theta)/\widetilde{F}_{11}^{\rm STMM}(\Theta)$ can be as low as 70%. Furthermore, the errors of the MG mixing rule now strongly depend on the host size parameter and can thus be expected to be significantly larger for dust particles with size parameters greater than 8. It appears that increasing x (while keeping the volume fraction of the inclusions constant) serves to decrease the extreme oscillations in the ratios $\widetilde{F}_{ij}^{\rm STMM}(\Theta)/\widetilde{F}_{11}^{\rm STMM}(\Theta)$ other than $\widetilde{F}_{22}^{\rm STMM}(\Theta)/\widetilde{F}_{11}^{\rm STMM}(\Theta)$ and to enhance the phase function at scattering angles between 80° and 160°. Furthermore, such effects of increasing heterogeneity as the side-scattering enhancement of the phase function and the growing deviation of the ratio $\widetilde{F}_{22}^{\rm STMM}(\Theta)/\widetilde{F}_{11}^{\rm STMM}(\Theta)$ from 100% appear to be sufficiently general to survive averaging over a polydispersion of aerosol sizes.

Table 2 also reveals a significant growth of errors of the MG mixing rules by the time the inclusion size parameter reaches the value $x = 0.5$ (the only exception is the error δg which remains small in the case of $X = 8$). Especially dramatic is the escalation of the error in the absorption cross section, $\delta C_{\rm abs}$. Interestingly, the MG mixing rule predicts absorption cross sections smaller than the exact STMM values. This trend is opposite to that observed for $X = 40$ water droplets contaminated by $x = 1$ soot inclusions [14].

5. Conclusions

Our analysis of the EMA differs from that by Liu et al. [15], Kahnert [16], and Videen et al. [27] who evaluated the numerical accuracy of mixing rules in cases selected on an *ad hoc* basis. Indeed, we first looked for the very existence of the effective medium regime under suitable conditions and then analyzed the result of an increasing violation of these conditions. In this way we have been able to confirm numerically that the EMA can indeed be realized in

the limit of a very small inclusion size parameter and a very low refractive-index contrast between the host and the inclusions. As these ideal conditions are increasingly violated, the accuracy of the EMA progressively deteriorates and eventually becomes inadequate.

In particular, we have been able to establish the existence of the effective-medium regime in the practically important cases of dust particles with hematite and air-bubble inclusions. The large refractive-index contrast between the host and inclusion materials in these cases necessitates extremely small inclusion size parameters for the EMA to work. We have not discussed specifically whether such small inclusions are indeed typical of real dust aerosols, but this issue should urgently be studied using modern laboratory instrumentation (cf. [12]). Obviously, finding that the actual size parameters of hematite and air-bubble inclusions in the near-UV, visible, and near-IR spectral ranges are substantially greater than a few tenths would cause a major modeling problem.

The results of Liu et al. [15] imply, qualitatively, that only in extremely well-mixed cases down to an inhomogeneity scale of $x \approx 0.4$ can the EMA be reliable, whereas the applicability of the EMA to cases of stratified or weak mixing is very limited (if not, in fact, fortuitous). Our results show that depending on the refractive-index contrast, the maximal allowable size parameter of the inclusions can be even smaller, especially in calculations of the scattering matrix and the absorption cross section. Furthermore, as the inclusion size parameter increases and approaches the threshold value, the scattering-matrix errors of the EMA start to grow with increasing the host size parameter and/or the number of the inclusions. This is another factor that must be taken into account in deciding whether to even attempt the use of a mixing rule.

Irrespective of the highly restricted conditions of applicability of the EMA, our numerically exact computer results provide further evidence that the effective-medium regime does exist, and this existence must follow from the fundamental laws of classical electromagnetics under quite specific assumptions. We hope that this additional evidence will stimulate attempts to derive the EMA as a direct corollary of the macroscopic Maxwell equations. This derivation can be expected to clarify the physical nature of the EMA as well as explain why its range of applicability appears to be so limited.

Acknowledgments

We thank Antti Penttilä for providing the upper panel of Fig. 1. This material is based upon work supported by the NASA Remote Sensing Theory Program managed by Lucia Tsaoussi. J.M.D. acknowledges support from the National Academy of Sciences of Ukraine under the Main Astronomical Observatory GRAPE/GPU/GRID Computing Cluster Project. A significant fraction of the numerical results reported in this paper were obtained with the "Discover" supercomputer at the NASA Center for Climate Simulation.

References

[1] Sihvola A. Electromagnetic mixing formulae and applications. London: IEE Press; 1999.

[2] Chýlek P, Videen G, Geldart DJW, Dobbie JS, Tso HCW. Effective medium approximations for heterogeneous particles. In: Mishchenko MI, Hovenier JW, Travis LD, editors. Light scattering by nonspherical particles: theory, measurements, and applications. San Diego: Academic Press; 2000. p. 273–308.

[3] Chianelli RR, Yácaman MJ, Arenas J, Aldape F. Atmospheric nanoparticles in photocatalitic and thermal production of atmospheric pollutants. J Hazard Subst Res 1998;1:1–17.

[4] Li J, Anderson JR, Busek PR. TEM study of aerosol particles from clean and polluted marine boundary layers over the North Atlantic. J Geophys Res 2003;108:4189.

[5] Li J, Pósfai M, Hobbs PV, Busek PR. Individual aerosol particles from biomass burning in southern Africa: 2. Compositions and aging of inorganic particles. J Geophys Res 2003;108:8484.

[6] Reid JS, Jonsson HH, Maring HB, Smirnov A, Savoie DL, Cliff SS, et al. Comparison of size and morphological measurements of coarse mode dust particles from Africa. J Geophys Res 2003;108:8593.

[7] Reid EA, Reid JS, Meier MM, Dunlap MR, Cliff SS, Broumas A, et al. Characterization of African dust transported to Puerto Rico by individual particle and size segregated bulk analysis. J Geophys Res 2003;108:8591.

[8] Chakrabarty RK, Moosmüller H, Garro MA, Arnott WP, Walker J, Susott RA, et al. Emissions from the laboratory combustion of wildland fuels: particle morphology and

size. J Geophys Res 2006;111:D07204.

[9] Chakrabarty RK, Beres ND, Moosmüller H, China S, Mazzoleni C, Dubey MK, et al. Soot superaggregates from flaming wildfires and their direct radiative forcing. Sci Rep 2014;4:5508.

[10] Adachi K, Chung SH, Buseck PR. Shapes of soot aerosol particles and implications for their effects on climate. J Geophys Res 2010;115:D15206.

[11] Adler G, Haspel C, Moise T, Rudich Y. Optical extinction of highly porous aerosol following atmospheric freeze drying. J Geophys Res Atmos 2014;119:6768–87.

[12] Jeong GY, Nousiainen T. TEM analysis of the internal structures and mineralogy of Asian dust particles and the implications for optical modeling. Atmos Chem Phys 2014;14:7233–54.

[13] Mishchenko MI, Liu L, Mackowski DW. Morphology-dependent resonances of spherical droplets with numerous microscopic inclusions. Opt Lett 2014;39:1701–4.

[14] Mishchenko MI, Liu L, Cairns B, Mackowski DW. Optics of water cloud droplets mixed with black-carbon aerosols. Opt Lett 2014;39:2607–10.

[15] Liu C, Panetta RL, Yang P. Inhomogeneity structure and the applicability of effective medium approximations in calculating light scattering by inhomogeneous particles. J Quant Spectrosc Radiat Transf 2014;146:331–48.

[16] Kahnert M. Modelling radiometric properties of inhomogeneous mineral dust particles: applicability and limitations of effective medium theories. J Quant Spectrosc Radiat Transf 2015;152:16–27.

[17] Videen G, Zubko E, Sun W, Shkuratov Yu. Mixing rules and morphology dependence of the scatterer. J Quant Spectrosc Radiat Transf 2015;150:68–75.

[18] Liu L, Mishchenko MI. Optics of water microdroplets with soot inclusions: exact versus approximate results. J Quant Spectrosc Radiat Transf 2016, this issue.

[19] Kahnert M. Numerical solutions of the macroscopic Maxwell equations for scattering by non-spherical particles: a tutorial review. J Quant Spectrosc Radiat Transf 2016, this issue.

[20] Lorentz HA. The theory of electrons. Leipzig: B. G. Teubner; 1916.

[21] Hoek H. Algemeene theorie der optische activiteit van isotrope media. Leiden: Leiden University; 1939.

[22] Rosenfeld L. Theory of electrons. Amsterdam: North-Holland; 1951.

[23] Jones DS. The theory of electromagnetism. Pergamon Press: Oxford; 1964.

[24] Russakoff G. A derivation of the macroscopic Maxwell equations. Am J Phys 1970;38:1188–95.

[25] Robinson FNH. Macroscopic electromagnetism. Oxford: Pergamon Press; 1973.

[26] van Kranendonk J, Sipe JE. Foundations of the macroscopic electromagnetic theory of dielectric media. Prog Opt 1977;15:245–350.

[27] Jackson JD. Classical electrodynamics. New York: Wiley; 1999.

[28] Brouder C, Rossano S. Microscopic calculation of the constitutive relations. Eur Phys J B 2005;45:19–31.

[29] Oughstun KE. Electromagnetic and optical pulse propagation. 1: Spectral representations in temporally dispersive media. New York: Springer; 2006.

[30] Silveirinha MG. Poynting vector, heating rate, and stored energy in structured materials: a first-principles derivation. Phys Rev B 2009;80:235120.

[31] Mishchenko MI, Dlugach ZhM, Zakharova NT. Direct demonstration of the concept of unrestricted effective-medium approximation. Opt Lett 2014;39:3935–8.

[32] Mishchenko MI, Travis LD, Lacis AA. Scattering, absorption, and emission of light by small particles. Cambridge: Cambridge University Press; 2002.

[33] Mishchenko MI. Electromagnetic scattering by particles and particle groups: an introduction. Cambridge: Cambridge University Press; 2014.

[34] Mackowski DW, Mishchenko MI. Calculation of the *T* matrix and the scattering matrix for ensembles of spheres. J Opt Soc Am A 1996;13:2266–78.

[35] Mackowski DW. A general superposition solution for electromagnetic scattering by multiple spherical domains of optically active media. J Quant Spectrosc Radiat Transf 2014;133:264–70.

[36] Mishchenko MI. Dlugach JM, Yurkin MA, Bi L, Cairns B, Liu L, et al. First-principle modeling of electromagnetic scattering by discrete and discretely heterogeneous

random media. 2016, submitted.

[37] van de Hulst HC. Light scattering by small particles. New York: Wiley; 1957.

[38] Lindqvist H, Jokinen O, Kandler K, Scheuvens D, Nousiainen T. Single scattering by realistic, inhomogeneous mineral dust particles with stereogrammetric shapes. Atmos Chem Phys 2014;14:143–57.

Table 1. Percent errors of the Maxwell-Garnett mixing rule.

m_{incl}	x	N	δC_{ext} (%)	δg (%)
1.4	0.3	8000	0.33	0.29
1.5	0.3	8000	0.67	0.40
1.6	0.3	8000	0.84	0.05
1.7	0.3	8000	0.57	–0.91
1.8	0.3	8000	–0.58	–1.63
1.9	0.3	8000	–2.34	–0.39
2	0.3	8000	–3.20	–0.91
1.4	0.6	1000	–5.96	–2.73

Table 2. Percent errors of the Maxwell-Garnett mixing rule in the case of dust aerosols with hematite inclusions.

X	x	N	δC_{ext} (%)	δC_{sca} (%)	δC_{abs} (%)	ϖ	$\delta\varpi$ (%)	δg (%)
4	0.1	1280	0.45	0.49	–5.14	0.9933	0.036	0.441
4	0.2	160	0.49	0.58	–14.49	0.9927	0.097	0.521
4	0.3	47	1.45	1.63	–25.33	0.9919	0.175	1.787
4	0.5	10	5.71	6.21	–72.15	0.9883	0.531	6.052
8	0.1	10240	0.05	0.12	–4.15	0.9842	0.065	–0.302
8	0.2	1280	0.09	0.30	–13.43	0.9827	0.209	–0.680
8	0.3	379	–0.19	0.22	–26.85	0.9808	0.411	–0.469
8	0.5	82	0.53	1.64	–71.62	0.9738	1.120	0.092

Table 3. Percent errors of the Maxwell-Garnett mixing rule in the case of dust aerosols with air-bubble inclusions.

X	x	N	δC_{ext} (%)	δg (%)
4	0.15	380	–0.10	–0.06
4	0.2	160	–0.53	–0.29
4	0.3	47	–0.42	–0.09
4	0.5	10	–0.24	0.52
4	1.09	1	0.34	1.11
8	0.15	3035	0.08	0.05
8	0.2	1280	–0.08	0.00
8	0.3	380	0.16	0.43
8	0.5	82	–0.52	0.54
8	1	11	–0.28	1.34

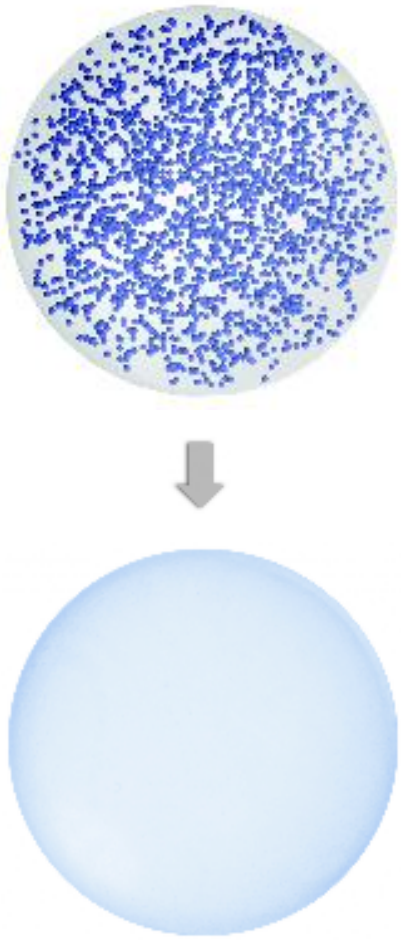

Figure 1. The essence of the effective-medium approximation.

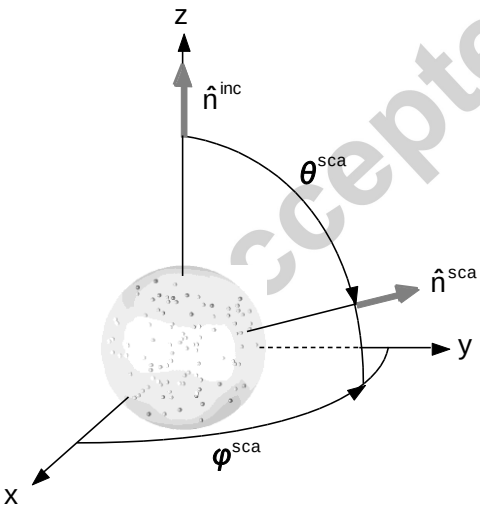

Figure 2. Scattering geometry.

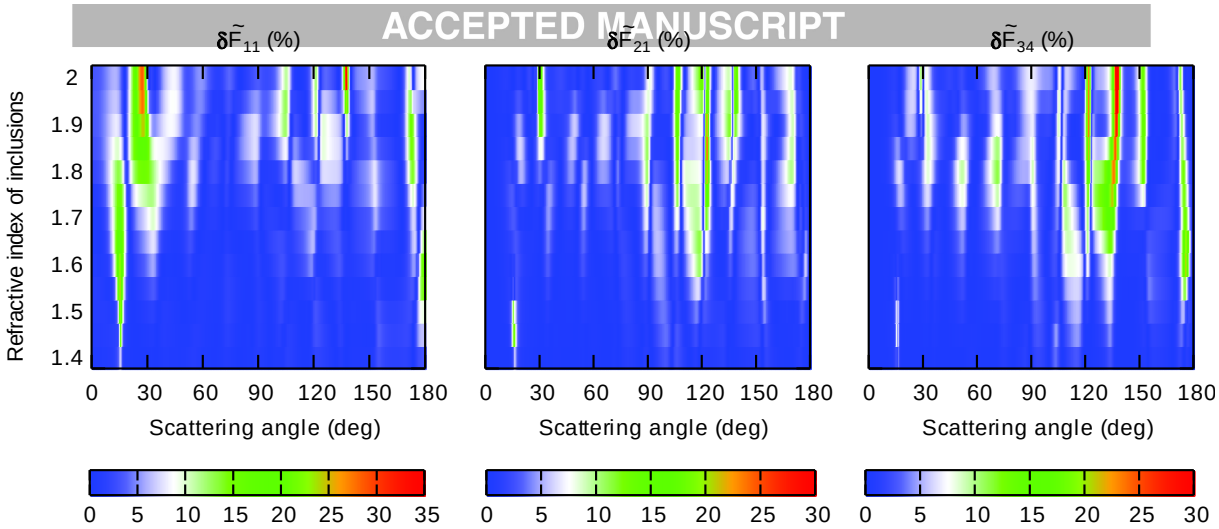

Figure 3. Percent errors of the Maxwell-Garnett mixing rule.

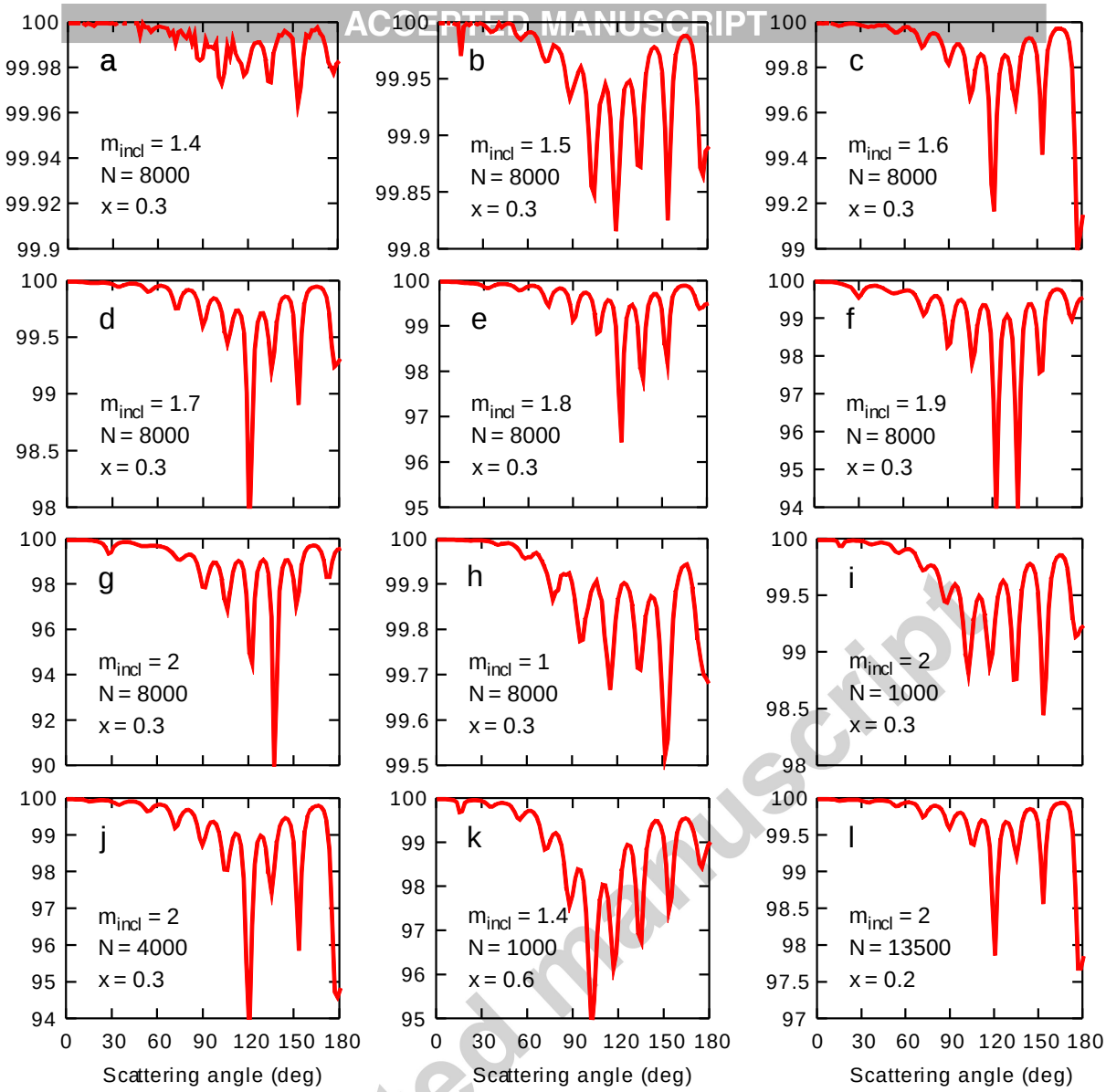

Figure 4. The ratio $\tilde{F}_{22}(\Theta)/\tilde{F}_{11}(\Theta)$ (in percent) for different models of a heterogeneous spherical particle.

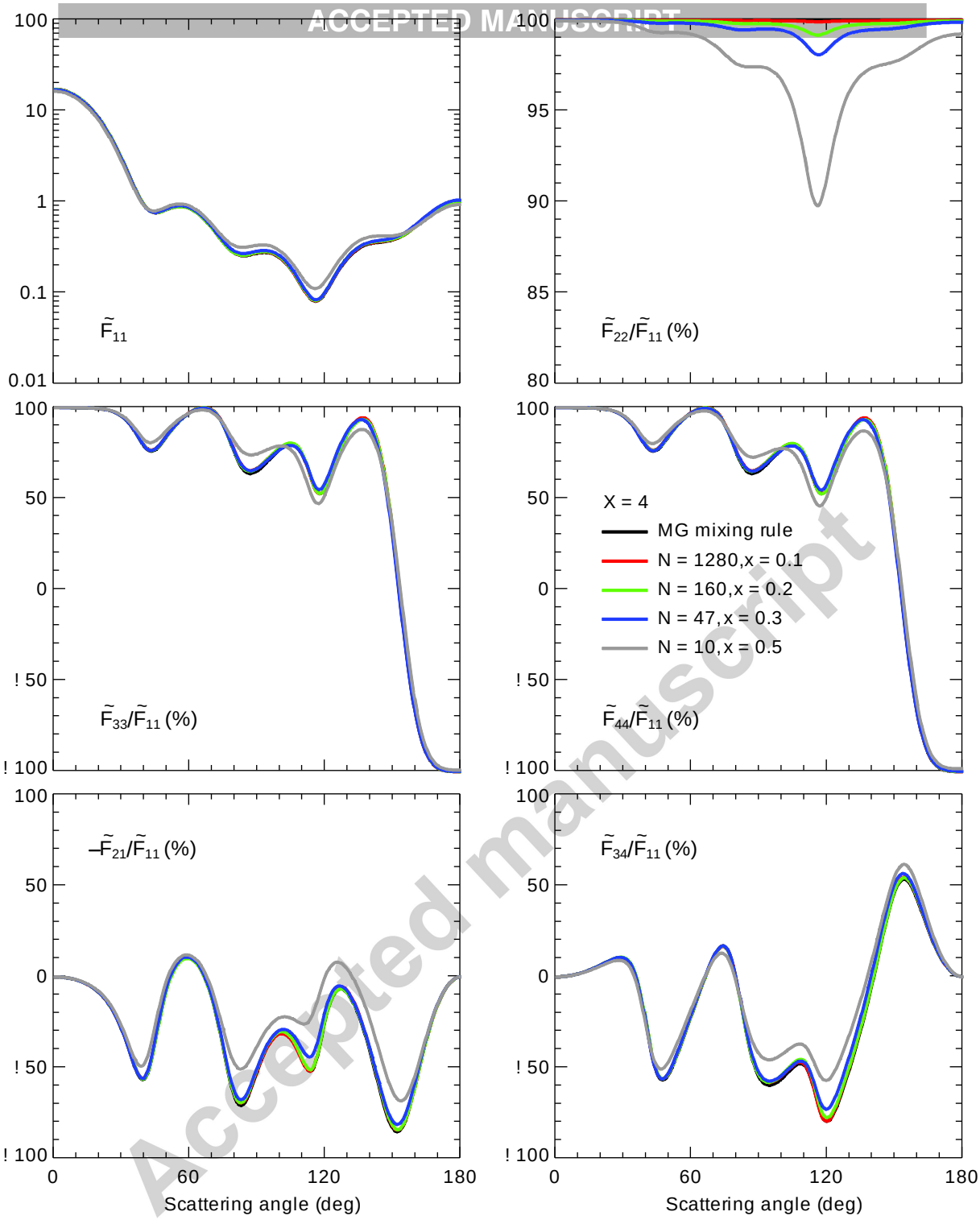

Figure 5. Elements of the dimensionless scattering matrix for X = 4 spherical dust particles filled with identical spherical hematite inclusions.

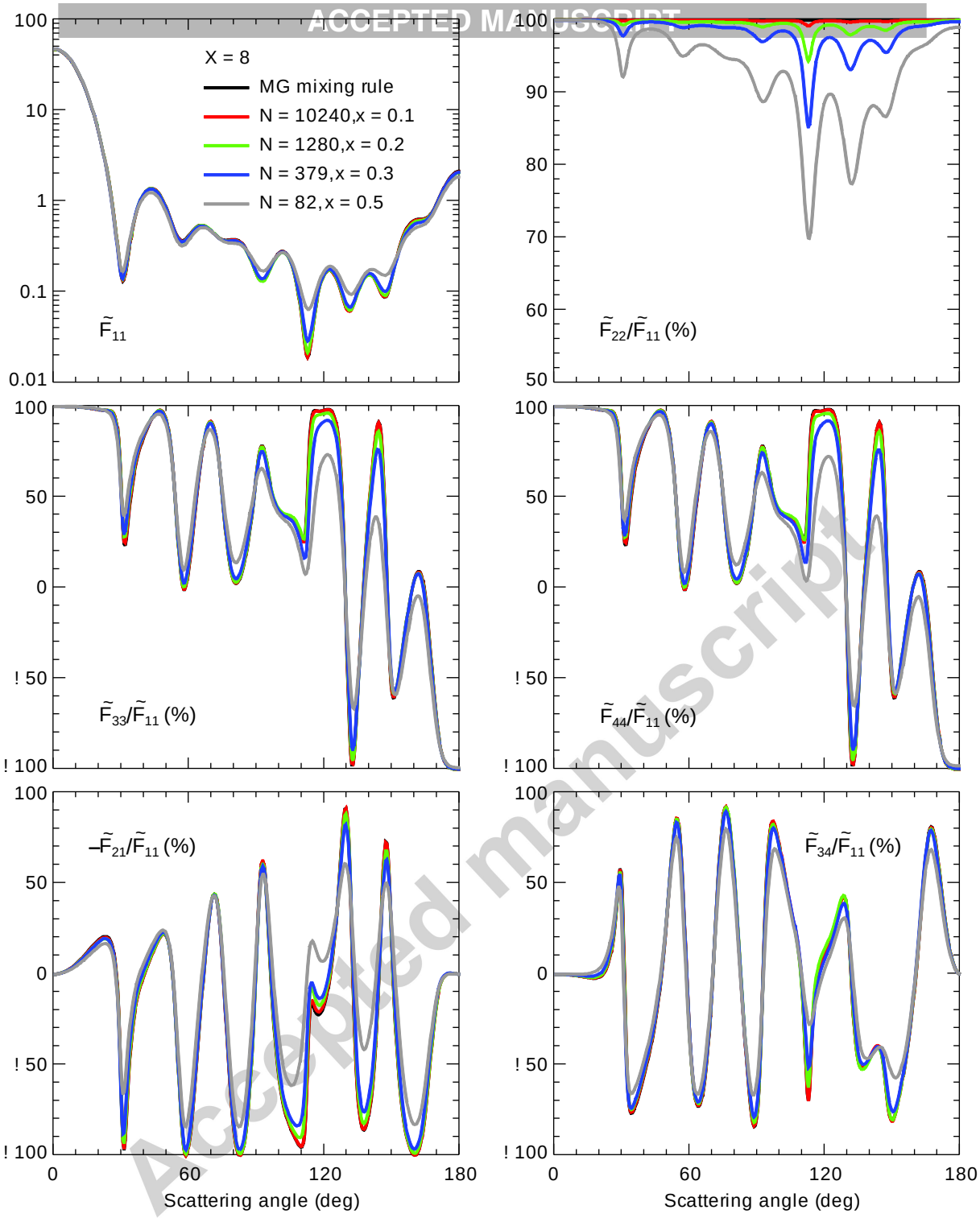

Figure 6. Elements of the dimensionless scattering matrix for X = 8 spherical dust particles filled with identical spherical hematite inclusions.

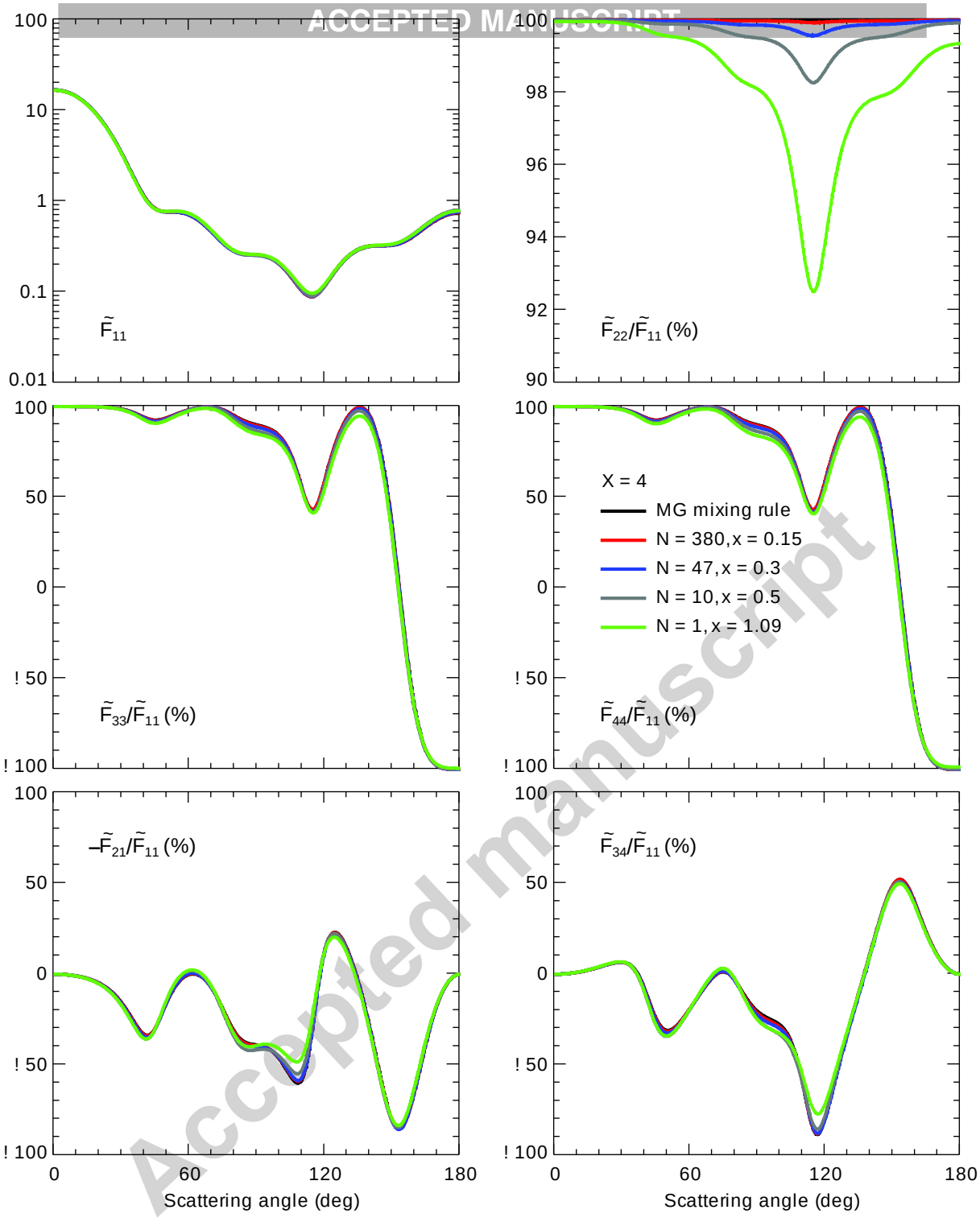

Figure 7. Elements of the dimensionless scattering matrix for X = 4 spherical dust particles filled with identical air-bubble inclusions.

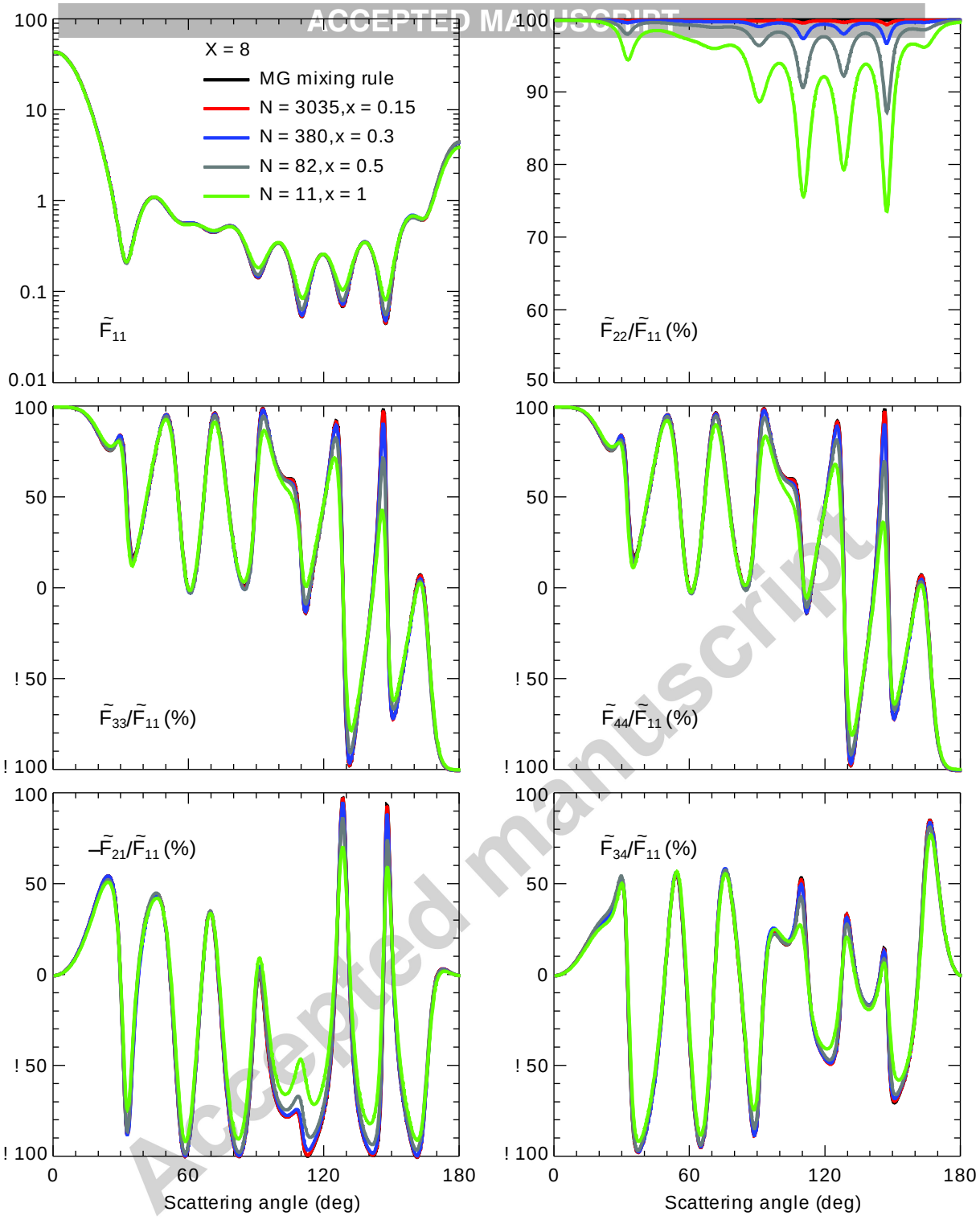

Figure 8. Elements of the dimensionless scattering matrix for X = 8 spherical dust particles filled with identical air-bubble inclusions.

Highlights

- Effective-medium regime can be realized for small inclusion size parameters.
- Threshold inclusion size parameter depends on the host and inclusion refractive indices.
- Effective-medium regime is confirmed for dust aerosols with hematite or air-bubble inclusions.
- Effective-medium regime must follow from the Maxwell equations under specific assumptions.